Uncertainty Estimation for Photogrammetric Point Clouds of UAV Imagery

Debao Huang[1,2,3], Rongjun Qin[1,2,3,4,*]

[1] Geospatial Data Analytics Laboratory, The Ohio State University, Columbus, USA - (huang.3918, qin.324)@osu.edu
[2] Department of Civil, Environmental and Geodetic Engineering, The Ohio State University, Columbus, USA
[3] Department of Electrical and Computer Engineering, The Ohio State University, Columbus, USA
[4] Translational Data Analytics Institute, The Ohio State University, Columbus, USA

Keywords: Uncertainty Estimation, Error Propagation, Dense Matching, Point Cloud, Unmanned Aerial Vehicle, Photogrammetry.

Abstract

Nowadays, unmanned aerial vehicles (UAVs) are widely used in various photogrammetric applications to collect high-resolution images for 3D reconstruction. Modern photogrammetric reconstruction often employs Structure-from-Motion (SfM) and Multi-View Stereo (MVS) to generate dense 3D point clouds from unordered image sets. Estimating the uncertainty of 3D point clouds is crucial, as it predicts error covariance matrices and indicates the reliability of the reconstructed point clouds. Despite its importance, little effort has been made to model uncertainty, particularly during the MVS stage, and to rigorously propagate uncertainties through the photogrammetric reconstruction process to the final 3D point clouds, leading to improper interpretation of their quality. Recent works on disparity uncertainty estimation also focus solely on stereo matching, ignoring the rich information provided by the MVS framework. In this work, we propose a novel method for estimating metric uncertainty in UAV imagery-derived 3D point clouds using error propagation. Specifically, we leverage multi-ray points from the MVS framework to map dense matching costs to metric disparity uncertainty. Our method requires no training data, making it generalizable to various UAV datasets. We evaluate our method on public and self-collected UAV datasets, and the results demonstrate that it outperforms existing approaches in terms of bounding rate.

1. Introduction

With the rapid advancement of unmanned aerial vehicles (UAVs) over the past decades, an increasing number of photogrammetry applications now utilize UAVs for tasks such as 3D modeling (Remondino et al., 2011; Xu et al.; Zhou et al., 2021), change detection (Andresen and Schultz-Fellenz, 2023; Xu et al., 2021), navigation (Han et al., 2024; Han et al., 2022; Lu et al., 2018), urban planning (Erenoglu et al., 2018; Kaya et al., 2023; Lu et al., 2023; Muhmad Kamarulzaman et al., 2023), agricultural monitoring (Liu et al., 2024; Marwah et al., 2023; Sahoo et al., 2023; Su et al., 2023), disaster monitoring (Erdelj and Natalizio, 2016; Wang et al., 2023), resource allocation (Lu et al., 2024; Xu et al., 2018), etc. UAVs are particularly favored in photogrammetric reconstruction due to their low cost, flexibility, and ability to capture high-resolution images. As shown in Figure 1, UAVs typically follow grid-like patterns when capturing images for 3D reconstruction. This approach ensures sufficient overlap for tie-point generation and provides greater redundancy in Bundle Adjustment (BA), which is crucial for achieving high reconstruction accuracy (Huang et al., 2022a; Huang et al., 2024). However, unlike other 3D reconstruction methods, such as airborne LiDAR (Chang et al., 2023; Elaksher et al., 2023), the accuracy of photogrammetric reconstruction is highly dependent on the scene. The accuracy of photogrammetric reconstruction can typically be assessed if ground truth (GT) reference data is available, such as ground control points (GCPs) (Martínez-Carricondo et al., 2018) or LiDAR-derived point clouds (Huang et al., 2022b; Wallace et al., 2016). In the research community, such GT data is often provided for evaluation. However, in real-world scenarios, data collection typically does not include a ground truthing step. Regardless of the availability of GT data, it is essential to understand the reliability of 3D point clouds, as it affects downstream data exploitation and analysis (Dolloff et al., 2024). Uncertainty estimation offers a comprehensive assessment of the quality and reliability of 3D point clouds by estimating and propagating uncertainty through each stage of the reconstruction process. The result of uncertainty estimation is a 3×3 covariance matrix for each 3D point in the final reconstruction, representing a general-shaped ellipsoid that indicates the potential error range in the 3D space, as shown in Figure 1. Two major sources of error arise from photogrammetric reconstruction, contributing to the uncertainty of 3D point clouds derived from images, particularly in the SfM and MVS stages. SfM estimates camera calibration, poses, and sparse point clouds, while MVS performs pairwise dense image matching and fuses the results to generate the final dense point clouds. Uncertainty estimation in the SfM stage has been well studied and standardized through BA using the Gauss-Markov Theorem

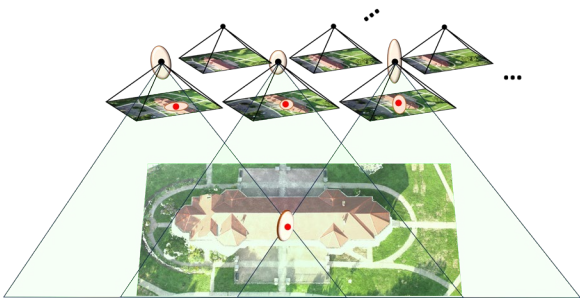

Figure 1 Data collection using UAVs and the resulting 3D point clouds. The uncertainty of each 3D point via error propagation is represented as a general-shaped ellipsoid.

* Corresponding author

(Thompson et al., 1966). However, the modeling of uncertainty in the MVS stage, as well as the rigorous propagation of these two error sources, remains underexplored. Previous works either omit modeling the uncertainty of the MVS stage or simply assign a fixed value, leading to unreasonable results and hindering the accurate interpretation of 3D point cloud quality. In recent years, a few efforts have been made to model disparity uncertainty. However, these approaches are primarily within the context of stereo matching, completely neglecting the valuable information provided by the MVS framework. Given that UAV datasets produce sufficient image overlap, this information could offer deeper insights into disparity uncertainty and, consequently, the uncertainty of the MVS stage. Thus, current approaches do not fully reflect the true quality of 3D point clouds, hindering the development of downstream data exploitation and analysis.

In this work, we present a novel method for estimating the uncertainty of UAV imagery-derived 3D point clouds through rigorous error propagation. The uncertainties of the SfM and MVS stages are estimated separately and propagated to the 3×3 covariance matrix of each 3D point in the final product. Specifically, we leverage multi-ray points from the MVS framework to estimate disparity uncertainty by mapping the matching cost (energy). Our method does not rely on training data, making it generalizable to various UAV datasets with sufficient overlap. We evaluate our method on both public and self-collected UAV datasets, comparing it with existing approaches. The results demonstrate that our method outperforms existing approaches in terms of bounding rates. The remainder of this paper is organized as follows: Section 2 reviews recent efforts in the research community, Section 3 presents our method for uncertainty estimation via error propagation, Section 4 provides a comprehensive evaluation, and Section 5 concludes with insights for future work.

2. Related Work

2.1 Structure-from-Motion

SfM is the process of recovering the 3D scene structure from a set of 2D images captured from different viewpoints of the scene. Most SfM approaches begin with feature extraction and matching, which can be either hand-crafted (Bay et al., 2008; Lowe, 2004) or learning-based (DeTone et al., 2018; Lindenberger et al., 2023; Sarlin et al., 2020). Geometric verification is then performed to filter out mismatched correspondences (Hartley and Zisserman, 2003). In incremental SfM approaches, which are widely used in photogrammetry applications, the 3D model is initialized with a two-view reconstruction from a carefully selected image pair (Beder and Steffen, 2006) and is gradually expanded by registering new cameras using PnP algorithms (Fischler and Bolles, 1981) and triangulating additional 3D points. BA is performed throughout the process to refine the reconstruction. Despite the critical role of camera calibration in SfM accuracy, most users only have access to manufacturer-provided calibration parameters or may even lack knowledge of these parameters altogether, while resources for rigorous camera calibration under laboratory conditions are scarce. Therefore, in recent SfM systems (Huang et al., 2024; Schonberger and Frahm, 2016), camera calibration is heuristically initialized if prior information is unavailable, and the camera’s intrinsic parameters are updated during BA through self-calibration.

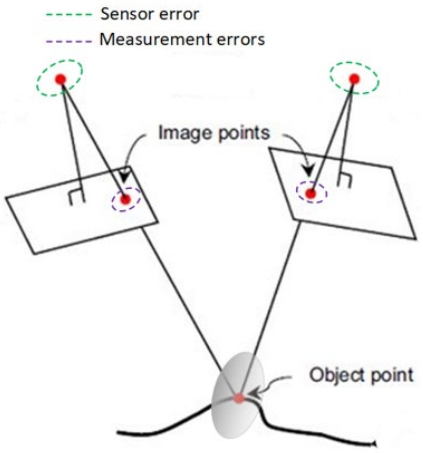

Figure 2 Overview of error propagation. In this work, we focus on the error propagation of sensor model errors and measurement errors.

2.2 Multi-View Stereo

Given a set of oriented images with overlaps from SfM, MVS performs stereo matching for each image pair and fuses the pairwise dense depth maps while enforcing multi-view consistency to generate the final dense 3D point cloud (Hartley and Zisserman, 2003). The work in (Seitz et al., 2006) introduces a taxonomy of multi-view stereo algorithms, categorizing them into four types: voxel-based methods, surface evolution-based methods, feature point growing-based methods, and depth-map fusion-based methods. Recent MVS frameworks and software (Cernea, 2020; Huang et al., 2022b; Remondino et al., 2022; Xu and Qin, 2024) predominantly adopt depth-map fusion-based methods due to their advantages in achieving finer geometry and better scalability. This type of approach typically employs either patch-based stereo matching (Barnes et al., 2009; Shen, 2013) or semi-global matching (SGM) (Hirschmuller, 2005, 2007) algorithms. Regardless of the differences in implementation, they all produce similar intermediate results, such as disparity maps and matching cost (energy) maps.

2.3 Uncertainty of Point Clouds

The National Geospatial-Intelligence Agency (NGA) proposed a community framework to model and store the uncertainty of each 3D point using the first-order statistics, called the Generic Point-cloud Model (GPM) (NGA, 2015). According to the official document, the sources of error primarily include sensor model errors, measurement errors, and unmodeled errors, as shown in Figure 2. Sensor model errors refer to the uncertainty in camera calibration and pose, which is carried out by BA in SfM. Measurement errors originally arise from an analyst’s ability to manually pick a point of interest. However, in the context of modern photogrammetry, where the reconstruction is automated through computer programs, measurement errors refer to errors in the dense image matching algorithm. Unmodeled errors consist of errors that cannot be practically characterized and are thus outside the scope of existing works.

While sensor model errors are well-studied and standardized in the literature through BA (Thompson et al., 1966), measurement errors remain largely underexplored. The process of stereo matching involves finding corresponding image points between two stereo images, which mimics the manual human measurement process. As a result, the disparity uncertainty can be propagated to the uncertainty of the final 3D point clouds.

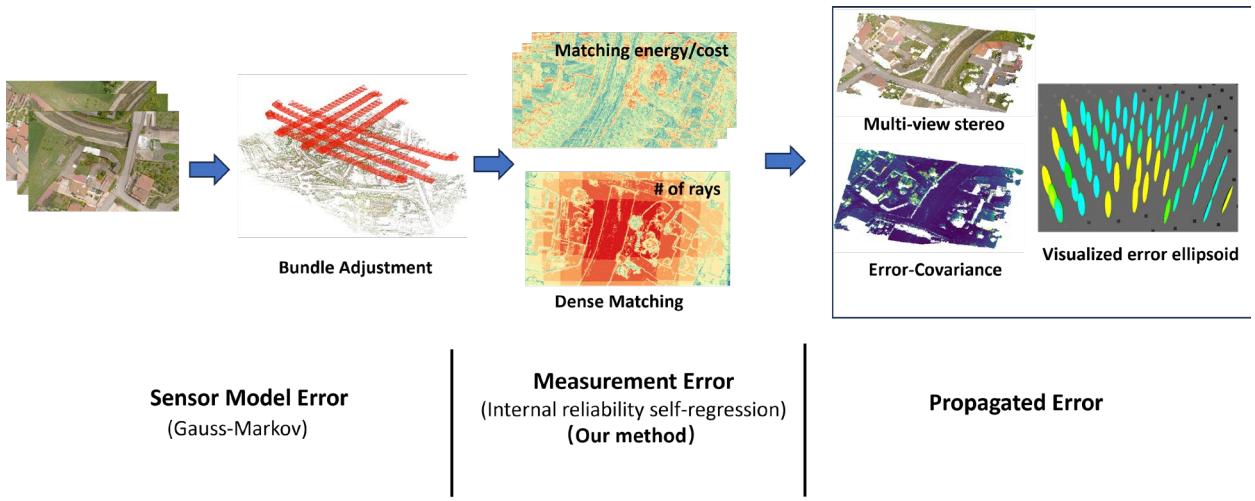

Figure 3 Overview of the pipeline. Our method leverages multi-ray points within the MVS framework to calibrate the magnitude of disparity uncertainty. The final results of error propagation can then be visualized as general-shaped ellipsoids.

Most existing works estimate the disparity uncertainty as a scalar between 0 and 1 (Hu and Mordohai, 2012; Veld et al., 2018), which lacks any actual unit and is not applicable for error propagation. In practice, it is typically assigned a fixed value, e.g., 2 pixels, which cannot comprehensively capture the varying uncertainty caused by different scenes. The series of works (Kuhn, 2014; Kuhn et al., 2017; Kuhn et al., 2014) introduce a novel perspective on disparity uncertainty estimation by leveraging the inherent properties so-called "total variation" (TV) of disparity maps. TV characterizes the local frequency around a pixel and assigns each pixel a class, which is then mapped to different disparity uncertainties in pixel units. It offers the advantages of being metric-based and applicable for error propagation. However, mapping TV classes to disparity uncertainties requires training data, which may exhibit significant domain differences from the actual processed data, leading to performance degradation. The derivation of TV is designed specifically for stereo matching, while valuable information from the MVS framework is overlooked even if UAV data typically has sufficient overlaps. On the contrary, our method eliminates the need for training data and utilizes multi-ray points from the MVS framework to self-calibrate disparity uncertainty.

3. Methodology

Figure 3 illustrates the pipeline for uncertainty estimation of UAV imagery-derived point clouds through error propagation. Specifically, we propose a novel method for estimating disparity uncertainty, built upon our preliminary study of reliable indicators of point cloud accuracy from the MVS framework (Huang and Qin, 2023). The results of preliminary study provide two key insights into the estimation of disparity uncertainty: 1) multi-ray ($n \geq 6$) points are more robust and stable in terms of accuracy. 2) dense image matching cost (or energy) is highly correlated with the accuracy of the final 3D points.

Our pipeline begins with the computation of sensor model errors, which are calculated using the Gauss-Markov theorem through BA in the SfM stage. Next, we perform a depth-map fusion-based MVS algorithm, which applies SGM to find dense correspondences between each stereo pair, resulting in disparity maps and, subsequently, depth maps. The dense image matching cost (energy) maps are retained as intermediate results, where the cost is formulated as the following equation:

$$E = \sum_{p} \left(C(p, D_p) + \lambda \sum_{q \in N_p} S(D_p, D_q) \right) \quad (1)$$

where C is the matching cost (energy) for pixel p associated with disparity value D_p, and $S()$ computes the smoothness of the neighborhood N_p surrounding pixel p. The ratio between the cost term and the smoothness term is controlled by the coefficient λ. For the reference view, each stereo pair formed by the reference image and one of the source images produces a depth map, which is then fed into the multi-view fusion process. A 3D point is generated only if it has a depth value in at least two depth maps, meaning it is visible from at least three views. The coordinates of the 3D point are the result of median filtering applied to all the available depth maps. As a result, when reprojecting the final 3D point back to each stereo pair, the reprojected pixel may differ from the dense correspondences found by the SGM algorithm.

Based on our previous findings (Huang and Qin, 2023), we select a subset of 3D points that are visible in at least six views and compute the reprojection errors of these points for each stereo pair. For each stereo pair, the joint distribution of dense image matching cost (energy) and reprojection errors of these multi-ray points is then established. These pixels are categorized into groups based on matching cost ranges, within which the standard deviation of projection errors is calculated to determine the disparity uncertainty for each group of pixels:

$$f: \bar{E}_i \mapsto \sigma_i \quad (2)$$

where $\bar{E}_i$ represents the mean matching cost of the pixels in group i. σ_i denotes the standard deviation of reprojection errors for the pixels in group i, which is equivalent to disparity uncertainty. f defines the mapping between matching cost and disparity uncertainty. To estimate the disparity uncertainty for the entire disparity map, each pixel is iterated through, and its matching cost is used to map to the disparity uncertainty using the closest group.

Once the disparity uncertainty is obtained for each stereo pair, constituting the measurement errors in the MVS stage, our pipeline proceeds with propagating both sensor model errors and measurement errors to the final 3D point clouds. We follow the protocol in GPM to estimate the uncertainty of the 3D point clouds:

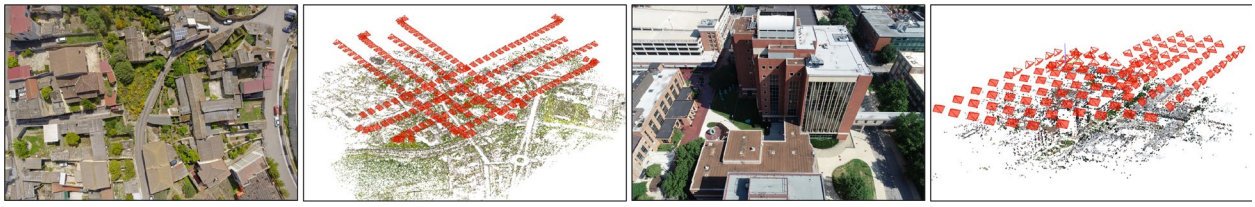

(a) UseGeo (b) OSU campus

Figure 4 Overview of datasets. Left: Sample image. Right: Sparse reconstruction results.

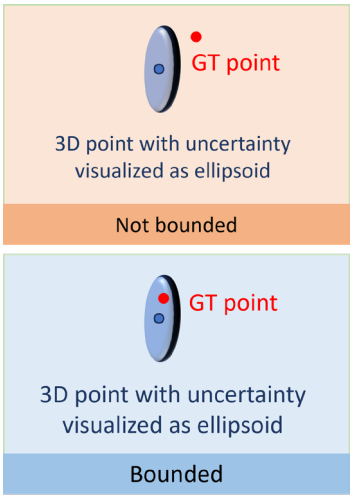

Figure 5 Illustration of the bounding rate. A point is considered bounded if its ground truth counterpart lies within the ellipsoid defined by the predicted covariance matrix.

$$\Sigma_g = (B_X^T(\Sigma_{sensor} + \Sigma_{measurement})^{-1}B_X)^{-1} \quad (3)$$

where Σ_g is a $3 * 3$ covariance matrix of a 3D point, B_X is a $2N * 3$ Jacobian matrix of 2D pixels w.r.t 3D point modeled by the projection function, Σ_{sensor} and $\Sigma_{measurement}$ are $2N * 2N$ covariance matrices from sensor model errors and measurement errors. Eq. 3 propagates the uncertainty from SfM and MVS in pixel unit to the uncertainty of 3D point clouds in meter unit.

4. Experimental Results

In this section, we present the details of the experiments and provide an analysis of the results.

4.1 Dataset

We conduct experiments to evaluate the performance of our uncertainty estimation method using two UAV datasets: the publicly available UseGeo datasets (Nex et al., 2024; Nex et al., 2023) and the self-collected OSU campus datasets. Figure 4 shows the overview of the two datasets. The UseGeo dataset contains approximately 200–300 images for each testing site, with LiDAR point clouds available as reference data. All images are captured at nadir angles. We select a subset of images from one site for our evaluation. The OSU campus dataset consists of approximately 100 images captured at both nadir and oblique angles. A subset of images capturing the main building is selected for evaluation.

Method	Bounding rate ↑
Confidence-based	N/A
TV-based	61%
Ours	67%

Table 1 Quantitative evaluation of uncertainty estimation for 3D point clouds.

	1x	2x	3x
Bounding rate ↑	67%	83%	91%

Table 2 Bounding rates with respect to different scaling factors of the predicted uncertainty.

4.2 Evaluation Setup

We select the confidence-based method (Veld et al., 2018) and the TV-based method (Kuhn et al., 2017) as baselines for comparison. The former is a representative method of confidence based approaches, leveraging the properties of the cost curve to predict the quality of stereo matching as a scalar between 0 and 1. The latter is a representative metric-based approach, as discussed in Section 2.3.

The experiments are conducted by running the photogrammetric reconstruction pipeline, as shown in Figure 3. The dense 3D point clouds are aligned to the LiDAR point clouds using the iterative closest point (ICP) algorithm (Besl and McKay, 1992; Xu et al., 2023). The actual error of each 3D point is measured as the distance between the point and a plane fitted to its six nearest neighbors in the LiDAR point cloud. To evaluate the performance of error propagation, we use the bounding rate as the evaluation metric, as depicted in Figure 5. Since the correspondences between the dense 3D point clouds and LiDAR point clouds are unknown, the bounding rate is defined as the percentage of 3D points whose actual error is smaller than the predicted uncertainty, which is represented by the norm of the covariance matrix. It is formulated as the following equation:

$$\rho = \frac{N_{bounded}}{N_{all}} \quad (4)$$

where $N_{bounded}$ is the number of 3D points which are bounded by the predicted uncertainty, N_{all} is the total number of 3D points.

4.3 Results and Analysis

UseGeo. Table 1 presents the statistical results of the evaluation on the UseGeo datasets. It can be seen that the confidence based method is not applicable for error propagation, as it produces a non-metric scalar. Our proposed method achieves a higher bounding rate than the TV-based method, thanks to its self-supervised nature and ability to leverage valuable information from the MVS framework. The UseGeo dataset features a high overlap during data collection (approximately 80%), providing sufficient multi-ray points to establish the mapping between

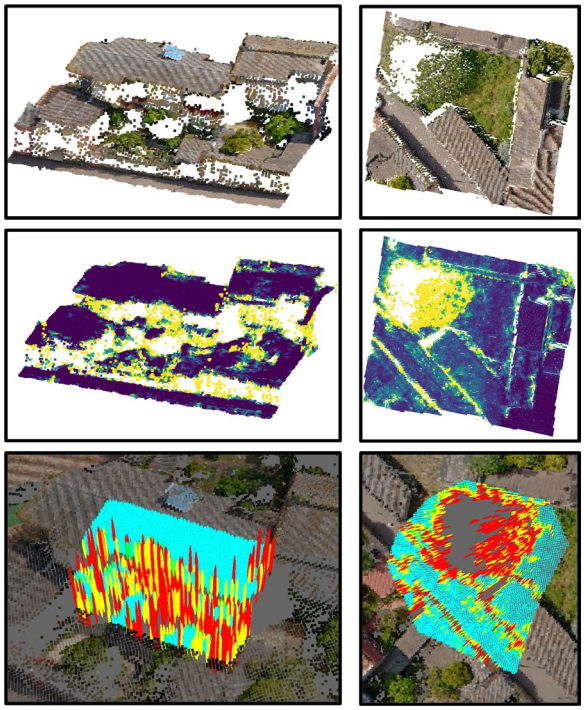

Figure 6 Visualization of the estimated uncertainty in 3D point clouds from the UseGeo dataset. First row: photogrammetric point clouds. Second row: estimated uncertainty of 3D point clouds. Third row: uncertainty visualization in ellipsoids.

dense image matching cost (energy) and disparity uncertainty. On the contrary, the TV-based method is largely constrained by the domain gap between its training dataset and the UseGeo dataset. The training dataset consists of a single indoor dataset collected in a lab setting, whereas the UseGeo dataset comprises outdoor UAV imagery.

We further scale the predicted uncertainty obtained using our proposed method by factors of 2 and 3. As shown in Table 2, this significantly enhances the bounding rate performance. It should be noted that there is a trade-off between the bounding rate and the meaningfulness of uncertainty estimation. A high bounding rate can be achieved by scaling up the predicted uncertainty; however, this leads to overestimation, making the values less informative about the actual quality of the 3D points.

The qualitative results of our method are depicted in Figure 6. It can be seen that facade regions and trees exhibit significantly higher uncertainty due to limited coverage in nadir images, occlusions, and the presence of thin structures, which are represented by larger (red) ellipsoids in the visualization. On the contrary, the roofs and ground regions exhibit lower uncertainty due to the presence of more distinct textures, which facilitate dense image matching and consequently result in lower measurement errors. In the visualization, this is represented by smaller (Cyan) ellipsoids.

OSU Campus. Additionally, we perform error propagation using our method on a self-collected UAV dataset of the OSU campus. Figure 7 presents the visualization results for the building facades and skybridge. The ellipsoids in these regions are significantly larger than those on the ground, indicating higher uncertainty due to the camera angle. Even though oblique images were captured during data collection, the lower half of the building facade remains farther from the UAV camera, while occlusions occur

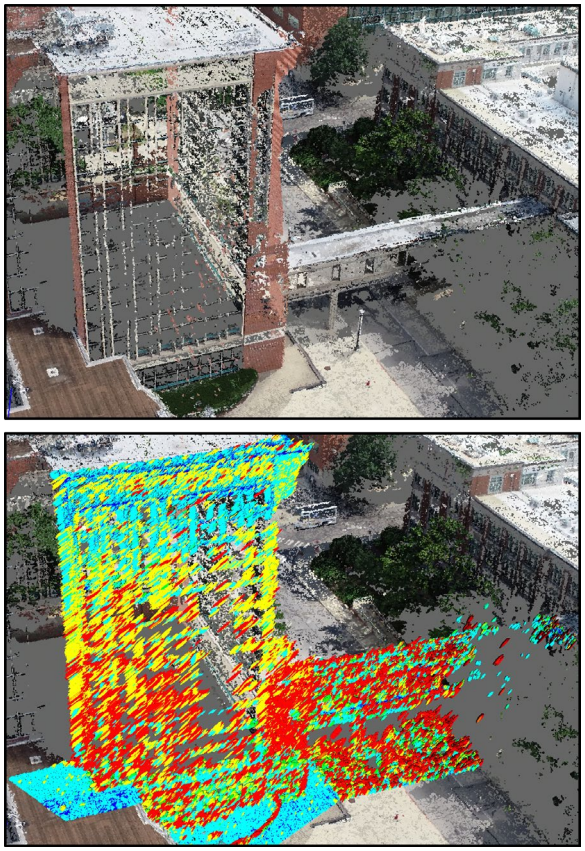

Figure 7 Visualization of the estimated uncertainty in 3D point clouds from the OSU campus dataset. First row: photogrammetric point clouds. Second row: uncertainty visualization in ellipsoids.

beneath the skybridge. We also observe that the dominant orientation of the ellipsoids aligns with the camera viewing angles: in the UseGeo dataset, where all images are captured at nadir angles, the ellipsoids are predominantly vertical, whereas in the OSU campus dataset, they tilt to coincide with the camera angles of the oblique images.

The experimental results demonstrate that our proposed method outperforms existing approaches in terms of bounding rate. It is also effective at capturing regions that potentially exhibit higher uncertainty. Additionally, our method accurately reflects the dominant direction of uncertainty, as the ellipsoids align with the direction of ray intersection.

5. Conclusion

In this paper, we introduce a novel method for estimating uncertainty that leverages the rich information available from the MVS setup in UAV imagery. Our proposed method offers the advantages of predicting metric uncertainty and being self-supervised, making it adaptable to existing MVS algorithms and various UAV datasets. The evaluation results on both public and self-collected UAV datasets demonstrate that our method achieves better performance in bounding rates and accurately reflects the uncertainty based on the scene and camera setup. The proposed uncertainty estimation method can facilitate various downstream applications in photogrammetry, such as weighted point cloud fusion and salient point detection. Future work could focus on evaluating disparity uncertainty using suitable datasets. Additionally, the full covariance matrix could be assessed if a ground truth dataset with known correspondences is available.

Acknowledgements

This work was partially supported by the Office of Naval Research (ONR, Award No. N00014-20-1-2141 & N00014-2312670). The authors would like to acknowledge the provision of the UseGeo dataset by ISPRS.

References

Andresen, C.G., Schultz-Fellenz, E.S., 2023. Change Detection Applications in the Earth Sciences Using UAS-Based Sensing: A Review and Future Opportunities. Drones 7, 258.

Barnes, C., Shechtman, E., Finkelstein, A., Goldman, D.B., 2009. PatchMatch: A randomized correspondence algorithm for structural image editing. ACM Trans. Graph. 28, 24.

Bay, H., Ess, A., Tuytelaars, T., Van Gool, L., 2008. Speeded-up robust features (SURF). Computer vision and image understanding 110, 346-359.

Beder, C., Steffen, R., 2006. Determining an initial image pair for fixing the scale of a 3d reconstruction from an image sequence, Joint Pattern Recognition Symposium. Springer, pp. 657-666.

Besl, P.J., McKay, N.D., 1992. Method for registration of 3-D shapes, Sensor fusion IV: control paradigms and data structures. Spie, pp. 586-606.

Cernea, D., 2020. OpenMVS: Multi-View Stereo Reconstruction Library.

Chang, Y., Xiao, W., Coifman, B., 2023. Using spatiotemporal stacks for precise vehicle tracking from roadside 3D LiDAR data. Transportation research part C: emerging technologies 154, 104280.

DeTone, D., Malisiewicz, T., Rabinovich, A., 2018. Superpoint: Self-supervised interest point detection and description, Proceedings of the IEEE conference on computer vision and pattern recognition workshops, pp. 224-236.

Dolloff, J., Theiss, H., Bollin, B., 2024. Assessment, Specification, and Validation of a Geolocation System's Accuracy and Predicted Accuracy. Photogrammetric Engineering & Remote Sensing 90, 157-168.

Elaksher, A., Ali, T., Alharthy, A., 2023. A quantitative assessment of LiDAR data accuracy. Remote Sensing 15, 442.

Erdelj, M., Natalizio, E., 2016. UAV-assisted disaster management: Applications and open issues, 2016 international conference on computing, networking and communications (ICNC). IEEE, pp. 1-5.

Erenoglu, R.C., Erenoglu, O., Arslan, N., 2018. Accuracy assessment of low cost UAV based city modelling for urban planning. Tehnički vjesnik 25, 1708-1714.

Fischler, M.A., Bolles, R.C., 1981. Random sample consensus: a paradigm for model fitting with applications to image analysis and automated cartography. Communications of the ACM 24, 381-395.

Han, Y., Toth, C., Yilmaz, A., 2024. Uas visual navigation in large and unseen environments via a meta agent. ISPRS Annals of the Photogrammetry, Remote Sensing and Spatial Information Sciences 10, 105-112.

Han, Y., Wei, J., Yilmaz, A., 2022. UAS Navigation in the Real World Using Visual Observation, 2022 IEEE Sensors. IEEE, pp. 1-4.

Hartley, R., Zisserman, A., 2003. Multiple view geometry in computer vision. Cambridge university press.

Hirschmuller, H., 2005. Accurate and efficient stereo processing by semi-global matching and mutual information, 2005 IEEE Computer Society Conference on Computer Vision and Pattern Recognition (CVPR'05). IEEE, pp. 807-814.

Hirschmuller, H., 2007. Stereo processing by semiglobal matching and mutual information. IEEE Transactions on pattern analysis and machine intelligence 30, 328-341.

Hu, X., Mordohai, P., 2012. A quantitative evaluation of confidence measures for stereo vision. IEEE transactions on pattern analysis and machine intelligence 34, 2121-2133.

Huang, D., Elhashash, M., Qin, R., 2022a. Constrained bundle adjustment for structure from motion using uncalibrated multi-camera systems. ISPRS Ann. Photogramm. Remote Sens. Spatial Inf. Sci. V-2-2022, 17-22. doi.org/10.5194/isprs-annals-V-2-2022-17-2022

Huang, D., Qin, R., 2023. A critical analysis of internal reliability for uncertainty quantification of dense image matching in multi-view stereo. ISPRS Annals of Photogrammetry, Remote Sensing and Spatial Information Sciences 1, 517-524.

Huang, D., Qin, R., Elhashash, M., 2024. Bundle adjustment with motion constraints for uncalibrated multi-camera systems at the ground level. ISPRS Journal of Photogrammetry and Remote Sensing 211, 452-464.

Huang, D., Tang, Y., Qin, R., 2022b. An evaluation of PlanetScope images for 3D reconstruction and change detection–experimental validations with case studies. GIScience & Remote Sensing 59, 744-761.

Kaya, Y., Şenol, H.İ., Yiğit, A.Y., Yakar, M., 2023. Car detection from very high-resolution UAV images using deep learning algorithms. Photogrammetric Engineering & Remote Sensing 89, 117-123.

Kuhn, A., 2014. Scalable 3D surface reconstruction by local stochastic fusion of disparity maps. Universitätsbibliothek der Universität der Bundeswehr München.

Kuhn, A., Hirschmüller, H., Scharstein, D., Mayer, H., 2017. A tv prior for high-quality scalable multi-view stereo reconstruction. International Journal of Computer Vision 124, 2-17.

Kuhn, A., Mayer, H., Hirschmüller, H., Scharstein, D., 2014. A TV prior for high-quality local multi-view stereo reconstruction, 2014 2nd International Conference on 3D Vision. IEEE, pp. 65-72.

Lindenberger, P., Sarlin, P.-E., Pollefeys, M., 2023. Lightglue: Local feature matching at light speed, Proceedings of the IEEE/CVF International Conference on Computer Vision, pp. 17627-17638.

Liu, J.-k., Qin, R., Arundel, S.T., 2024. Assessing the utility of uncrewed aerial system photogrammetrically derived point clouds for land cover classification in the Alaska North Slope. Photogrammetric Engineering & Remote Sensing 90, 405-414.

Lowe, D.G., 2004. Distinctive image features from scale-invariant keypoints. International journal of computer vision 60, 91-110.

Lu, J., Feng, W., Pu, D., 2024. Resource Allocation and Offloading Decisions of D2D Collaborative UAVassisted MEC Systems. KSII Transactions on Internet & Information Systems 18.

Lu, J., Li, J., Yu, F.R., Jiang, W., Feng, W., 2023. UAV-Assisted Heterogeneous Cloud Radio Access Network with Comprehensive Interference Management. IEEE Transactions on Vehicular Technology.

Lu, Y., Xue, Z., Xia, G.-S., Zhang, L., 2018. A survey on vision-based UAV navigation. Geo-spatial information science 21, 21-32.

Martínez-Carricondo, P., Agüera-Vega, F., Carvajal-Ramírez, F., Mesas-Carrascosa, F.-J., García-Ferrer, A., Pérez-Porras, F.-J., 2018. Assessment of UAV-photogrammetric mapping accuracy based on variation of ground control points. International journal of applied earth observation and geoinformation 72, 1-10.

Marwah, N., Singh, V.K., Kashyap, G.S., Wazir, S., 2023. An analysis of the robustness of UAV agriculture field coverage using multi-agent reinforcement learning. International Journal of Information Technology 15, 2317-2327.

Muhmad Kamarulzaman, A.M., Wan Mohd Jaafar, W.S., Mohd Said, M.N., Saad, S.N.M., Mohan, M., 2023. UAV Implementations in Urban Planning and Related Sectors of Rapidly Developing Nations: A Review and Future Perspectives for Malaysia. Remote Sensing 15, 2845.

Nex, F., Stathopoulou, E., Remondino, F., Yang, M., Madhuanand, L., Yogender, Y., Alsadik, B., Weinmann, M., Jutzi, B., Qin, R., 2024. UseGeo-A UAV-based multi-sensor dataset for geospatial research. ISPRS Open Journal of Photogrammetry and Remote Sensing, 100070.

Nex, F., Zhang, N., Remondino, F., Farella, E., Qin, R., Zhang, C., 2023. Benchmarking the extraction of 3D geometry from UAV images with deep learning methods. International Archives of the Photogrammetry, Remote Sensing and Spatial Information Sciences 48, 123-130.

NGA, 2015. NGA Standardization Document. The Generic Point-cloud Model (GPM): Implementation and Exploitation (Rev. 2023-11-15) Version 1.1 ed.

Remondino, F., Barazzetti, L., Nex, F., Scaioni, M., Sarazzi, D., 2011. UAV photogrammetry for mapping and 3D modeling: Current status and future perspectives, Proceedings of the International Conference on Unmanned Aerial Vehicle in Geomatics (UAV-g): 14-16 September 2011, Zurich, Switzerland. International Society for Photogrammetry and Remote Sensing (ISPRS), pp. 25-31.

Remondino, F., Morelli, L., Stathopoulou, E., Elhashash, M., Qin, R., 2022. Aerial triangulation with learning-based tie points. The International Archives of the Photogrammetry, Remote Sensing and Spatial Information Sciences 43, 77-84.

Sahoo, R.N., Gakhar, S., Rejith, R., Ranjan, R., Meena, M.C., Dey, A., Mukherjee, J., Dhakar, R., Arya, S., Daas, A., 2023. Unmanned aerial vehicle (UAV)–based imaging spectroscopy for predicting wheat leaf nitrogen. Photogrammetric Engineering & Remote Sensing 89, 107-116.

Sarlin, P.-E., DeTone, D., Malisiewicz, T., Rabinovich, A., 2020. Superglue: Learning feature matching with graph neural networks, Proceedings of the IEEE/CVF conference on computer vision and pattern recognition, pp. 4938-4947.

Schonberger, J.L., Frahm, J.-M., 2016. Structure-from-motion revisited, Proceedings of the IEEE conference on computer vision and pattern recognition, pp. 4104-4113.

Seitz, S.M., Curless, B., Diebel, J., Scharstein, D., Szeliski, R., 2006. A comparison and evaluation of multi-view stereo reconstruction algorithms, 2006 IEEE computer society conference on computer vision and pattern recognition (CVPR'06). IEEE, pp. 519-528.

Shen, S., 2013. Accurate multiple view 3d reconstruction using patch-based stereo for large-scale scenes. IEEE transactions on image processing 22, 1901-1914.

Su, J., Zhu, X., Li, S., Chen, W.-H., 2023. AI meets UAVs: A survey on AI empowered UAV perception systems for precision agriculture. Neurocomputing 518, 242-270.

Thompson, M.M., Eller, R.C., Radlinski, W.A., Speert, J.L., 1966. Manual of photogrammetry. American Society of Photogrammetry Falls Church, VA.

Veld, R.O.H., Jaschke, T., Bätz, M., Palmieri, L., Keinert, J., 2018. A novel confidence measure for disparity maps by pixel-wise cost function analysis, 2018 25th IEEE International Conference on Image Processing (ICIP). IEEE, pp. 644-648.

Wallace, L., Lucieer, A., Malenovský, Z., Turner, D., Vopěnka, P., 2016. Assessment of forest structure using two UAV techniques: A comparison of airborne laser scanning and structure from motion (SfM) point clouds. Forests 7, 62.

Wang, Y., Su, Z., Xu, Q., Li, R., Luan, T.H., Wang, P., 2023. A secure and intelligent data sharing scheme for UAV-assisted disaster rescue. IEEE/ACM Transactions on Networking 31, 2422-2438.

Xu, D., Sun, Y., Ng, D.W.K., Schober, R., 2018. Robust resource allocation for UAV systems with UAV jittering and user location uncertainty, 2018 IEEE Globecom Workshops (GC Wkshps). IEEE, pp. 1-6.

Xu, N., Huang, D., Song, S., Ling, X., Strasbaugh, C., Yilmaz, A., Sezen, H., Qin, R., 2021. A volumetric change detection framework using UAV oblique photogrammetry–a case study of ultra-high-resolution monitoring of progressive building collapse. International Journal of Digital Earth 14, 1705-1720.

Xu, N., Qin, R., 2024. Geospecific View Generation Geometry-Context Aware High-Resolution Ground View Inference from Satellite Views, European Conference on Computer Vision. Springer, pp. 349-366.

Xu, N., Qin, R., Huang, D., Remondino, F., Multi-tiling neural radiance field (NeRF)—geometric assessment on large-scale aerial datasets. The Photogrammetric Record.

Xu, N., Qin, R., Song, S., 2023. Point cloud registration for LiDAR and photogrammetric data: A critical synthesis and performance analysis on classic and deep learning algorithms. ISPRS open journal of photogrammetry and remote sensing 8, 100032.

Zhou, T., Lv, L., Liu, J., Wan, J., 2021. Application of UAV oblique photography in real scene 3d modeling. The International Archives of the Photogrammetry, Remote Sensing and Spatial Information Sciences 43, 413-418.